Supporting information

Nitride-based interfacial layers for monolithic tandem integration of new solar energy materials on Si: The case of CZTS

Filipe Martinho[1,*,†], Alireza Hajijafarassar[2,*,†], Simón Lopez-Marino[2], Moises Espíndola-Rodríguez[3], Sara Engberg[1], Mungunshagai Gansukh[1], Fredrik Stulen[4], Sigbjørn Grini[4], Stela Canulescu[1,*], Eugen Stamate[2], Andrea Crovetto[5], Lasse Vines[4], Jørgen Schou[1], Ole Hansen[2]

[1]Department of Photonics Engineering, Technical University of Denmark, DK-4000 Roskilde, Denmark.

[2]DTU Nanolab, Technical University of Denmark, DK-2800 Kgs. Lyngby, Denmark

[3]DTU Energy, Technical University of Denmark, DK-4000 Roskilde, Denmark.

[4]Department of Physics, University of Oslo, 0371 Oslo, Norway

[5]DTU Physics, Technical University of Denmark, DK-2800 Kgs. Lyngby, Denmark.

Corresponding Author

*Email: filim@fotonik.dtu.dk (Filipe Martinho), alhaj@dtu.dk (Alireza Hajijafarassar), stec@fotonik.dtu.dk (Stela Canulescu)

† - These authors contributed equally to this work

Results and Discussion (supplementary)

In the main text, it was mentioned that the barrier layer thickness (comparing the TiN-5 and TiN-10 cases) had no noticeable influence on the protection of the Si bottom cell, both in experiments with SiN patterning and without patterning. **Figure S1** shows a side-by-side Si lifetime comparison of two non-patterned tandem wafer pieces with 5 nm and 10 nm TiN, after CZTS annealing. The measurement was done on a full tandem wafer, before the Ag back contact deposition. The lifetime mapping shows comparable lifetime values. In both cases, the original Si lifetime (before CZTS processing) was slightly above 1 ms, meaning that a significant degradation occurred in both cases.

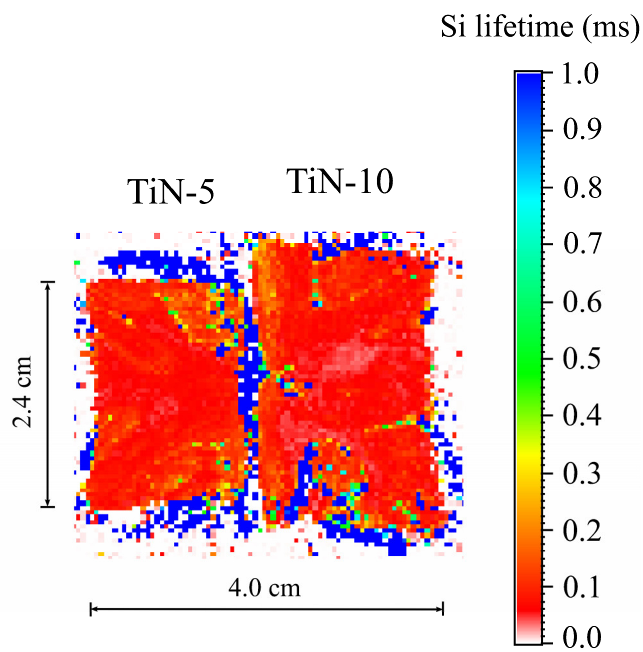

Figure S1 – Si minority carrier lifetime comparison for a TiN barrier layer thickness of 5 nm (left) and 10 nm (right). The annealing temperature for CZTS formation was 575 °C.

The data in **Figure S1** indicates that both TiN barriers have a temperature threshold lower than the CZTS annealing temperature used. In the main text, the TiN-5 case is used to analyze the effects of Si bottom cell degradation on the J-V and EQE results. In **Figure S2**, the TiN-10 results are added for comparison. The results are similar, but the lower transmittance of the TiN-10 barrier leads to an even lower Si cell EQE overall.

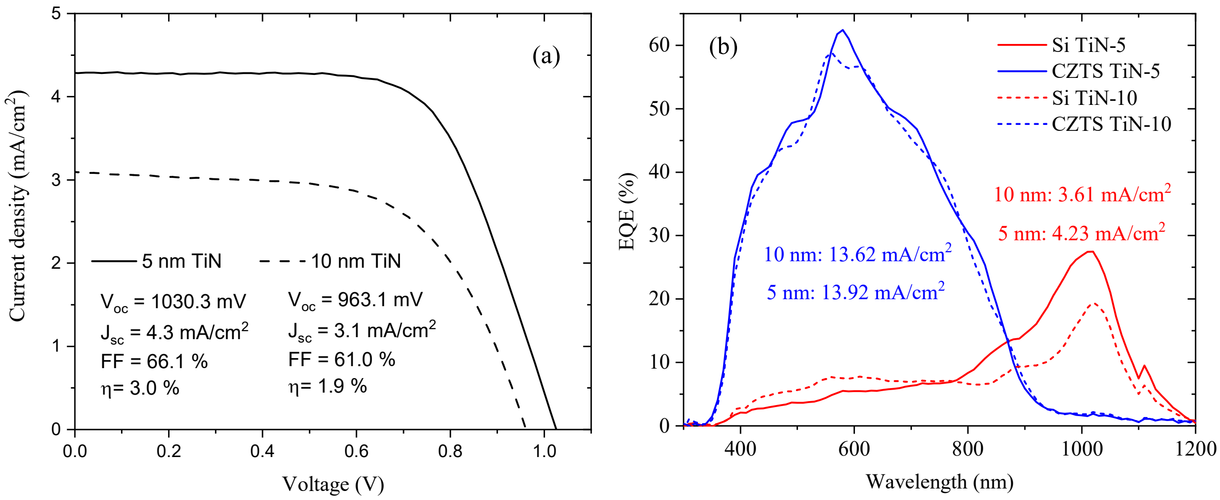

Figure S2 – (a) J-V characteristic curve and (b) EQE results of two CZTS/Si tandem cells with a 5 nm (solid line) and 10 nm (dashed line) TiN barrier layer (TiN-5 and TiN-10).

Another aspect discussed in the text was a slight tandem V_{oc} degradation occurring after cleaving the tandem cells. Due to the large area difference between typical Si cells and CZTS cells processed in our facilities (typically several cm^2 versus <1 cm^2, respectively), the full tandem cell was cleaved in several pieces, and the tandem cell area was defined by the geometry of the cleaving itself. However, cleaving a Si wafer into smaller sizes exposes its edges, and increases the edge area proportion relative to the total area, which can increase the surface recombination velocity and hence reduce the V_{oc} contribution from the Si bottom cell. We have found experimental evidence of this degradation, as shown in **Figure S3**. The highest V_{oc} measured in this case was 1064 mV before cleaving, for the TiN-5 case. A small difference in V_{oc} between the 5 nm and 10 nm is visible, with the TiN-5 case showing higher V_{oc}. Part of this difference is again explained by the differences in transmittance between the two barriers, but a small contribution can also be due to variations in the V_{oc} produced by the CZTS top cell. Nevertheless, according to **Figure S2 (b)**, the EQE of the CZTS top cells was quite comparable for this trial. These results suggest that the effective tandem cell V_{oc}s achievable with this configuration are well above 1V.

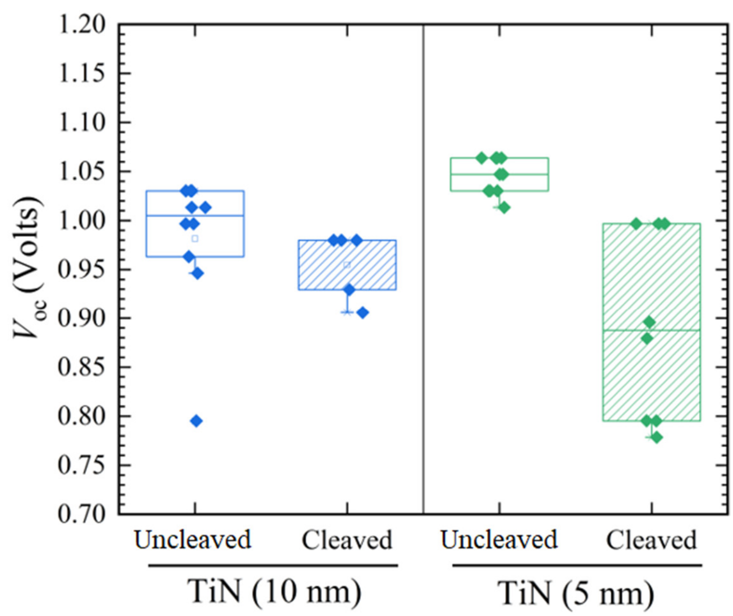

Figure S3 – Effect of cleaving on the total tandem cell V_{oc}. In all trials, the uncleaved area was on the order of a few cm^2, whereas after cleaving the area is reduced to below 1 cm^2.

To analyze and interpret the decrease in performance of the Si bottom cell after CZTS annealing, as shown from the J-V and EQE results of the main text and from **Figure S2**, we propose the following simple theoretical model. The external quantum efficiency (EQE) of a cell with window layer with transmittance T and reflectance R is $\text{EQE} = (1 - R)T\text{IQE}$, where IQE is the internal quantum efficiency, defined as the spectrally resolved ratio of collected current density $J_C(\lambda)$ to incident photon flux density $J_{\gamma 0}(\lambda)$ on the absorber (after reflection) multiplied by the unit charge q, i.e.,

$$\text{IQE}(\lambda) = \frac{J_C(\lambda)}{qJ_{\gamma 0}(\lambda)} \tag{1}$$

The photon flux density $J_\gamma(x, \lambda)$ in the absorber decays exponentially with depth x into the absorber $J_\gamma(x, \lambda) = J_{\gamma 0}(\lambda) \exp(-\alpha x)$ due to absorption characterized by the absorption coefficient $\alpha = \alpha(\lambda)$ of the absorber. The absorption causes in turn an electron-hole pair generation rate $G(x, \lambda) = \alpha J_\gamma(x, \lambda)$,[1] and some fraction $C_E(x)$ of the generated minority carriers reach the separating junction, where they are collected and add to the collected current, i.e., the incremental current density $\mathrm{d}J_C$ from the absorber element $\mathrm{d}x$ at x is

$$\mathrm{d}J_C(x, \lambda) = qC_E(x)\alpha(\lambda)J_\gamma(x, \lambda)\,\mathrm{d}x \tag{2}$$

where $C_E(x)$ is the collection efficiency/probability. It follows that the incremental $\mathrm{dIQE} = \mathrm{d}J_C(x, \lambda)/\left[qJ_{\gamma 0}(\lambda)\right]$ is

$$\mathrm{dIQE} = C_E \alpha \exp(-\alpha x)\,\mathrm{d}x \tag{3}$$

since the common factor $J_{\gamma 0}(\lambda)$ cancels out. Thus, the internal quantum efficiency is obtained from the integral over the thickness L of the absorber

$$\text{IQE} = \int_0^L C_E \alpha \exp(-\alpha x)\,dx \tag{4}$$

Based on this expression for the IQE, we will consider a few model cases next. The collection efficiency/probability C_E is easily calculated using Donolato's reciprocity theorem,[2,3] which essentially says that the charge collection probability equals the excess carrier profile for a unit excess carrier injection at the charge collection junction. Therefore, the corresponding hole continuity equation becomes:

$$\frac{\partial p}{\partial t} = D\frac{d^2 p}{dx^2} - \frac{p - p_0}{\tau_{\text{bulk}}} \tag{5}$$

where the excess carrier concentration $p - p_0$ is defined as the collection efficiency C_E, τ_{bulk} is the bulk lifetime and D is the diffusion coefficient. Using the diffusion length $L_p = \sqrt{D\tau_{\text{bulk}}}$ and considering the steady-state solution, the equation to consider is then

$$\frac{d^2 C_E}{dx^2} - \frac{C_E}{L_P^2} = 0 \tag{6}$$

In our sample, we consider a perfectly collecting junction at $x = L$, so the boundary condition is $C_E(L) = 1$. We shall include interface recombination at the illuminated surface $x = 0$, with recombination velocity S, therefore the surface boundary condition is $D\frac{dC_E}{dx}(0) = SC_E(0)$. Then, the solution for the collection probability C_E (excess carrier profile) is

$$C_E(x) = \frac{\sinh\left(\frac{x}{L_p}\right) + \frac{D}{SL_p}\cosh\left(\frac{x}{L_p}\right)}{\sinh\left(\frac{L}{L_p}\right) + \frac{D}{SL_p}\cosh\left(\frac{L}{L_p}\right)} \tag{7}$$

Neglecting bulk recombination first, then $L_p \gg L$, and we can make the approximation

$$C_E(x) \approx \left(\frac{x}{L} + \frac{D}{SL}\right) \Big/ \left(1 + \frac{D}{SL}\right) \tag{8}$$

In the ideal case, $C_E = 1$, and then the integral yields

$$\text{IQE}^{\text{ideal}} = 1 - \exp(-\alpha L) \tag{9}$$

In case of an extremely poor front surface (infinite surface recombination velocity) we have $C_E = x/L$, and thus

$$\text{IQE} = \int_0^L \frac{x}{L}\alpha \exp(-\alpha x)\, dx = \frac{1-\exp(-\alpha L)}{\alpha L} - \exp(-\alpha L) \tag{10}$$

Finally, in the general case (still without bulk recombination) the IQE integral is

$$\text{IQE} = \int_0^L \frac{\frac{x}{L} + \frac{D}{SL}}{1+\frac{D}{SL}}\alpha \exp(-\alpha x)\, dx \tag{11}$$

with solution

$$\text{IQE} = \frac{\frac{D}{SL}(1-\exp(-\alpha L)) + \frac{1-\exp(-\alpha L)}{\alpha L} - \exp(-\alpha L)}{1+\frac{D}{SL}} \tag{12}$$

The solutions to this **Equation (12)** for different values of *S* and *L* are plotted in **Figure S4 (a)** and **(b)**.

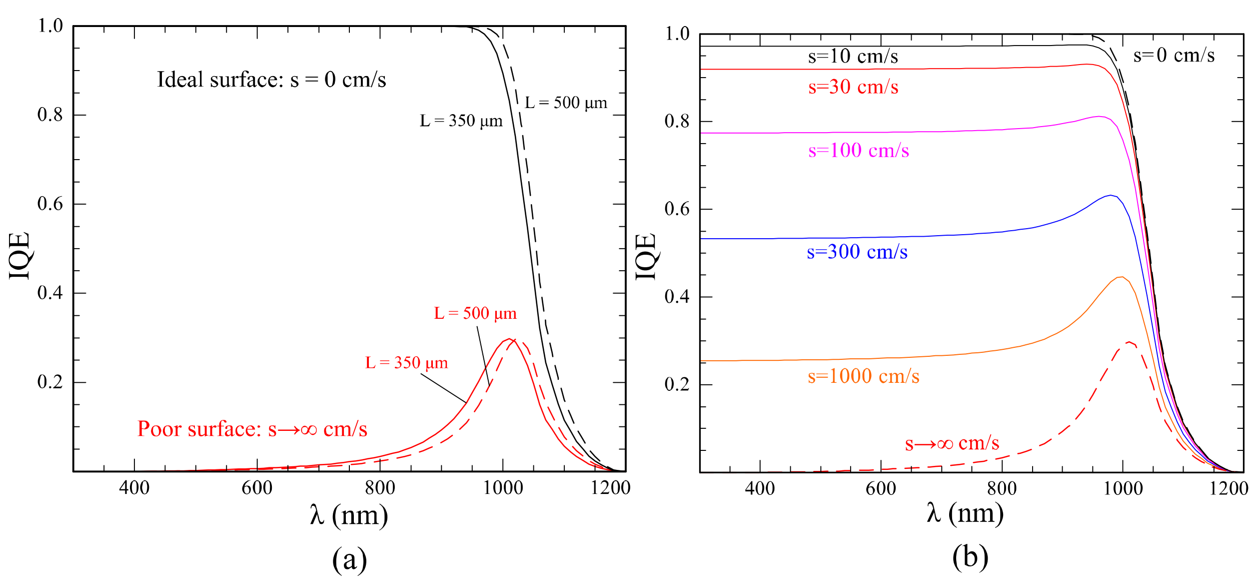

Figure S4 – Calculated internal quantum efficiency for (a) ideal and poor surface cases, where the dashed curves correspond to a cell thickness L = 500 µm and the full curves correspond to L = 350 µm, and (b) different surface recombination velocities for L = 350 µm.

When considering simultaneously bulk and interface recombination, we must solve the integral

$$\mathrm{IQE} = \int_0^L \frac{\frac{\mathrm{SL_p}}{D}\sinh\left(\frac{x}{L_p}\right) + \cosh\left(\frac{x}{L_p}\right)}{\frac{\mathrm{SL_p}}{D}\sinh\left(\frac{L}{L_p}\right) + \cosh\left(\frac{L}{L_p}\right)} \alpha \exp(-\alpha x)\, dx \tag{13}$$

Which has the solution

$$\mathrm{IQE} = \frac{\alpha L_p}{2} \frac{\left(\frac{\mathrm{SL_p}}{D} + 1\right)\frac{e^{-\alpha L} e^{\frac{L}{L_p}} - 1}{1 - \alpha L_p} + \left(\frac{\mathrm{SL_p}}{D} - 1\right)\frac{e^{-\alpha L} e^{-\frac{L}{L_p}} - 1}{1 + \alpha L_p}}{\left(\cosh\left(\frac{L}{L_p}\right) + \frac{\mathrm{SL_p}}{D}\sinh\left(\frac{L}{L_p}\right)\right)} \tag{14}$$

Equation (14) was then used in the main text to simulate IQE curves for typical effective lifetime values of compromised Si bottom cells (10, 30 and 50 μs, in **Figure 5**). The shape of the solutions obtained from the simulations resemble the EQE of the Si bottom cell in the tandem cell results shown in the main text. However, the presence of the CZTS top cell and its absorption convolutes the results and complicates the analysis. Therefore, we have fabricated single junction Si solar cells where CZTS was fabricated on top of Si as in the main text (co-sputtering + annealing in sulfur), and subsequently CZTS and TiN were selectively removed by chemical etching in a mixture of H_2O_2:4H_2SO_4 (piranha) and RCA1 solutions, followed by a dilute HF dip. The Si cells, with an area of 0.8 x 0.8 cm^2 were fabricated from a quarter section of a wafer comparable to the wafer with a barrier layer of 10 nm TiN (TiN-10 from the main text), and also 25 nm TiN. Al-doped ZnO (AZO) was used as the front electrode. The contact area between CZTS and TiN/Si was defined through a 75 nm SiN patterned window, similar to the patterned window experiment shown in the main text. A photograph of the wafer is shown in **Figure S5**. The quarter used for a single junction Si cell after CZTS processing is labelled "*CZTS Reference piece*"

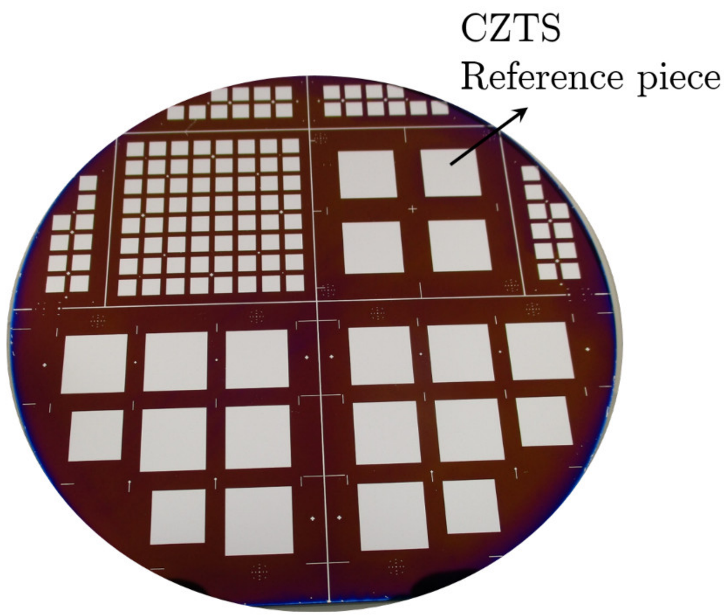

Figure S5 – The patterned wafer used for tandem fabrication in the main text. The dark blue/brown color is due to SiN patterning. The highlighted piece was used to evaluate the possible effects of CZTS processing on the performance of the bottom silicon cell.

The corresponding lifetime results after CZTS annealing are shown in **Figure S6**. The results are very similar to those shown in the main text for the SiN-patterned wafer (**Figure 1** of the main text), showing that the thicknesses here used – 25, 10 and 5 nm – had very little effect on the barrier properties, for the TiN barrier case. The loss in lifetime is caused mainly by a loss in surface passivation after CZTS processing, with a corresponding increase in surface recombination velocity.

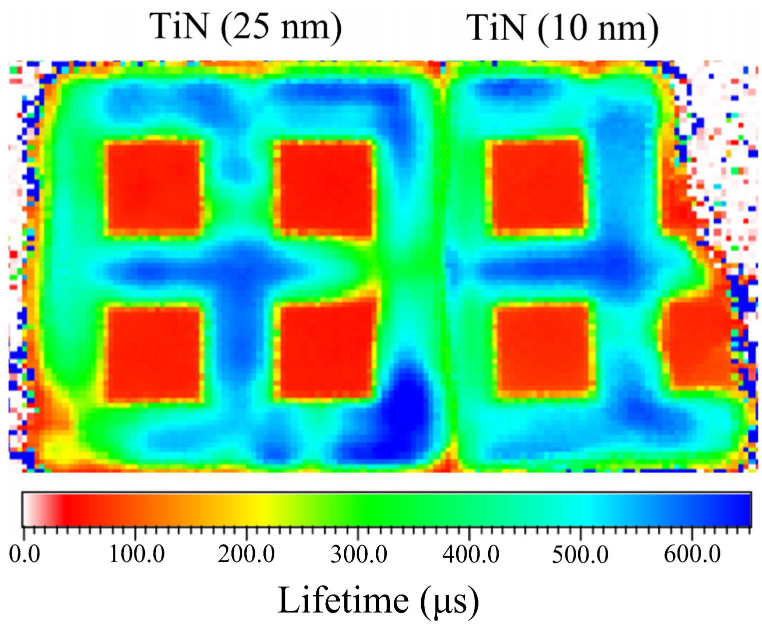

Figure S6 – Lifetime map of the pieces used for single junction Si cell fabrication after CZTS annealing. The squares (shown in red) are the points of contact between CZTS and TiN/Si as defined by the windows in the 75 nm SiN. The left piece had a TiN barrier of 25 nm, while the right piece had a TiN barrier of 10 nm (the TiN-10 case of the main text).

The corresponding EQE of the single junction Si solar cells is shown in **Figure S8**. A *Reference* is added corresponding to a standard TOPCon Si solar cell, without any CZTS or TiN processing. Compared to the *Reference*, the pieces which underwent CZTS processing show a very poor peak EQE and poor short wavelength response, similar to the theoretical prediction of our model (**Figure S4 (a)** and **(b)**, and **Figure 5** of the main text), and in line with the corresponding lifetime results of **Figure S7**.

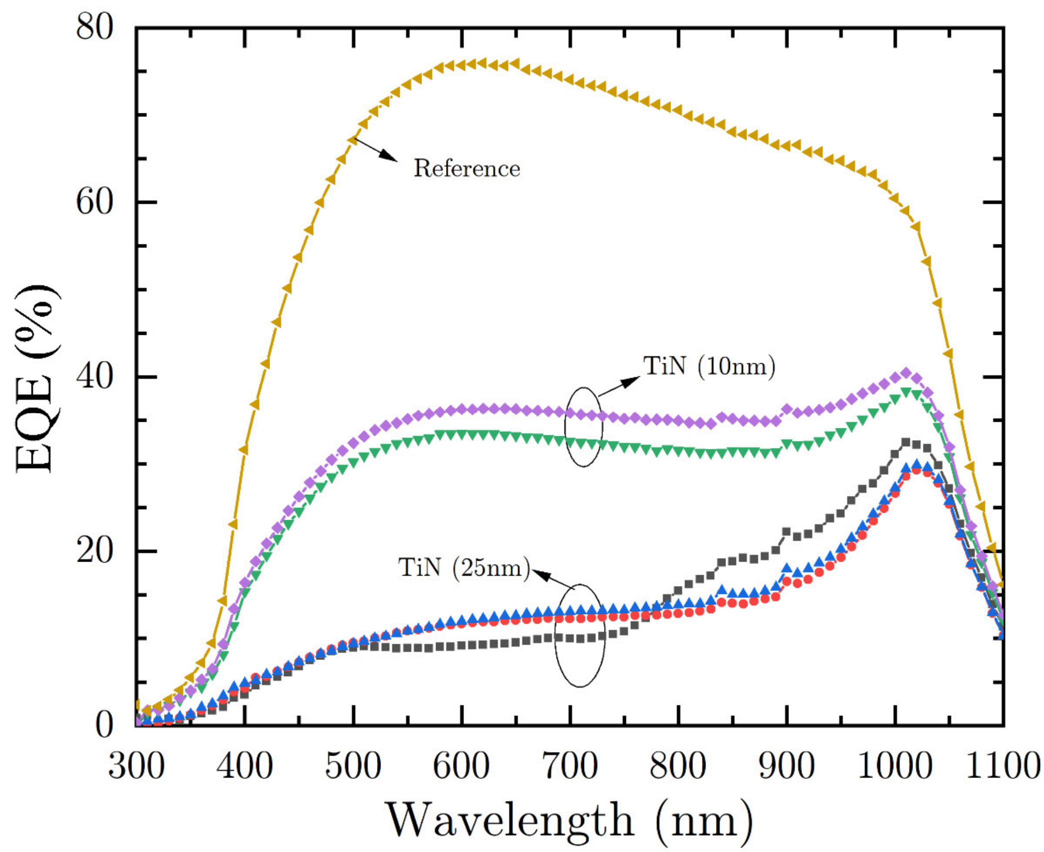

Figure S8 – EQE of single junction Si cells, made from the *CZTS Reference Piece*, compared with a standard Si cell reference where no CZTS or TiN processing was done. The poor low wavelength response in samples with CZTS processing is an indication of a loss of surface passivation quality, resulting in an increase in surface recombination velocity.

From the results of **Figure S8**, it could seem that the 25 nm TiN barrier was inferior to the 10 nm barrier, which would be counterintuitive since it is a thicker barrier. However, as we have shown in **Figure 5** of the main text, for very compromised Si bottom cells, a small variation in effective lifetime can cause large variations in the IQE. Such small variations (all compromised samples are in a range of a few tens of μs) are not representative of the effect of the barrier, but of spontaneous sample-to-sample and process variability. Comparing the 25, 10 and 5 nm cases

(**Figure S8** and **Figure S9 (b)**) further shows that there is no trend with thickness. In all three cases, the barrier layer failure leads to a two order of magnitude decrease in lifetime (from 1 ms to a range of 10-50 μs). Note that, additionally, in **Figure S10 (b)** the difference between the 5 and 10 nm cases is also related to differences in transmittance between the TiN-5 and TiN-10 barriers.

In the main text, it was shown that the Si lifetime increases for lower annealing temperatures, as the temperature gets closer to the threshold of the barrier layers. Unfortunately, at the same time, our baseline CZTS efficiency progressively deteriorates as the annealing temperature decreases, as shown in **Figure S11**. This ultimately means that the TiN-5 and TiN-10 are poor barrier layers in the optimal temperature range found for fabricating the CZTS top cell. In the case of the TiN-Al-10 barrier, the barrier performance was better, but still led to a partially compromised Si bottom cell. We note that this is the case for our CZTS fabrication procedure, but different groups have optimal conditions with slightly different temperature and annealing time. Furthermore, different top cell materials will require different synthesis conditions, which will pose specific contamination and diffusion issues to the Si bottom cell. The key here is to develop specific barrier layers adequate to each case, which maximize the compromise between optical transmittance, barrier quality and lossless interconnection between top cell and bottom cell.

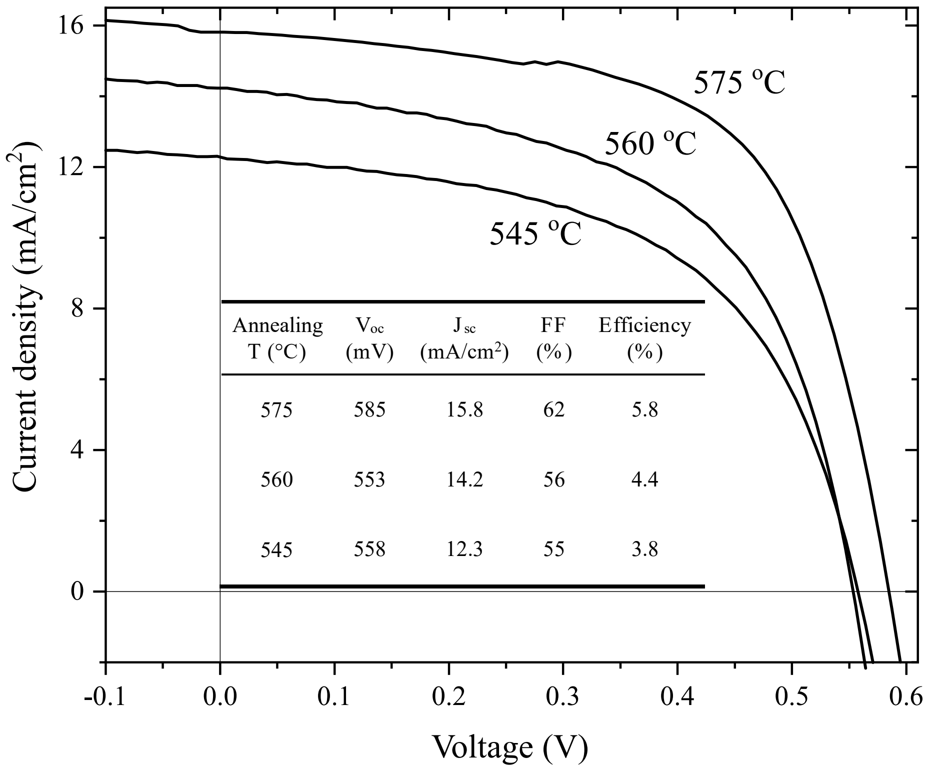

Annealing T (°C)	V_{oc} (mV)	J_{sc} (mA/cm²)	FF (%)	Efficiency (%)
575	585	15.8	62	5.8
560	553	14.2	56	4.4
545	558	12.3	55	3.8

Figure S11 – Efficiency of the baseline single junction CZTS solar cells used in this work for different annealing temperatures.

References

(1) Würfel, P.; Würfel, U. *Physics of Solar Cells: From Basic Principles to Advanced Concepts*, 3rd ed.; Wiley-VCH, 2016.

(2) Donolato, C. A Reciprocity Theorem for Charge Collection. *Appl. Phys. Lett.* **1985**, *46* (3), 270–272. https://doi.org/10.1063/1.95654.

(3) Donolato, C. Reciprocity Theorem for Charge Collection by a Surface with Finite Collection Velocity: Application to Grain Boundaries. *J. Appl. Phys.* **1994**, *76* (2), 959–966. https://doi.org/10.1063/1.357774.